Electropreconcentration diagrams to optimize molecular enrichment with low counter pressure in a nanofluidic device

Sokhna-mery Ngom, Fatima Flores-galicia, François-damien Delapierre, Antoine Pallandre, Jean Gamby, Isabelle Le Potier, Anne-Marie Haghiri-Gosnet

Electropreconcentration diagrams to optimize molecular enrichment with low counter pressure in a nanofluidic device.

Journal:	*ELECTROPHORESIS*
Manuscript ID	Draft
Wiley - Manuscript type:	Research Paper
Date Submitted by the Author:	n/a
Complete List of Authors:	Ngom, Sokhna-Mery; C2N, Microsystems and Nanobiofluidics Flores-Galicia, Fatima; C2N, Microsystems and Nanobiofluidics Delapierre, François-Damien; C2N, Microsystems and Nanobiofluidics Pallandre, Antoine; Laboratoire de chimie physique d'Orsay, Chemistry Gamby, Jean; C2N, Microsystems and Nanobiofluidics Le Potier, Isabelle; C2N, Microsystems and Nanobiofluidics Haghiri-Gosnet, Anne-Marie; C2N, Microsystems and Nanobiofluidics
Keywords:	Nanofluidics, Electrokinetic transport, Preconcentration diagrams

Electropreconcentration diagrams to optimize molecular enrichment with low counter pressure in a nanofluidic device.

Sokhna-Mery Ngom[a], Fatima Flores-Galicia[a], François-Damien Delapierre[a], Antoine Pallandre[b⊥], Jean Gamby[a⊥], Isabelle Le Potier[a⊥] and Anne-Marie Haghiri-Gosnet[a].*

[a] Centre de Nanosciences et Nanotechnologies C2N, CNRS, Université Paris-Saclay, UMR9001, 10 Boulevard Thomas Gobert, 91120 Palaiseau, France

[b] Université Paris-Saclay, CNRS, Institut de Chimie Physique, UMR8000, 91405 Orsay, France

[⊥]*These authors have equally contributed to the paper.*

Abstract:

Ion-concentration-polarization (ICP) - based focusing electrokinetics nanofluidic devices have been developed in order to simultaneously detect and enrich very diluted analytes on chip. However, stabilization of focal points over long time under the application of the electric field remains as a technical bottleneck. If pressure-assisted preconcentration methods have been proposed to stabilize propagating modes at $^1/_{D_u} \ll 1$, these recent protocols remain laborious for

optimizing experimental parameters. We report "field/pressure" E/P diagrams for fluorescein where the typical regimes, i.e. propagating focusing, stable focusing and stacking can be observed. The region of stable focusing is shown to vary depending of the nanoslit length (100µm < $L_{nanoslit}$ < 500µm) and the nature of the background electrolyte (BGE) (KCl and NaCl). Longer nanoslits (500µm) produce stabilization at low pressure, whereas NaCl BGE offers a narrower and more fluorescent stable window in the E/P diagram compared to KCl. Finally, the ability of such pressure-assisted protocol to concentrate negatively charged proteins has been tested with 10µM ovalbumin in HEPES and the corresponding E/P diagram for ovalbumin confirms the existence of a stable focusing regime at low electric field.

Keywords: Nanofluidics, Electrokinetic transport, Preconcentration diagrams

*Corresponding author: anne-marie.haghiri@c2n.upsaclay.fr
Co-corresponding author: antoine.pallandre@u-psud.fr

1. Introduction

In the field of highly sensitive biochemical analysis, Lab-on-a-Chip (LoC) devices have to face the challenge of maintaining a good level of sensitivity and selectivity, while decreasing the amount of analyte. The analysis of highly diluted biomarkers produced at the very early stages of a disease is always facing the issue of reaching the relevant sensitivity to provide a reliable diagnosis. It is therefore crucial to couple good separation with sensitive and specific detection [1]. Separation methods that consist in controlling the spatial location of the analyte in the fluid over time [2-7] may suffer from a lack of sensitivity since there is no preconcentration. In this context developing new solutions for sample analyte preconcentration in bioanalytical fluidic devices remains a necessity. To address this prevalent issue, many focusing techniques based on electrokinetic phenomena have been proposed, among which ion concentration polarization [8-20], field-amplified sample stacking (FASS) [21-23], concentration gradient focusing [24-27] and isoelectric focusing [28-30]. All these techniques allow focusing analytes by exploiting the unbalanced ionic transport between anionic and cationic species due to the competition between electroosmotic flow (EOF) and electrophoretic flow (EP).

This unbalanced transport under electric field is exacerbated in a nanofluidic device that integrates channels with at least one nanometric dimension [6]. In such nanofluidic device filled with a background electrolyte (BGE), this exacerbated unbalanced transport produces an enrichment-exclusion effect that is called the ion concentration polarization (CP) phenomenon [9-10]. This CP effect is mainly governed by the background electrolyte (BGE) concentration and the geometrical constraints imposed by the nanofluidic geometry. At each side of the nanochannel, CP generates BGE enrichment (cathodic reservoir) and depletion (anodic reservoir) zones with respectively a high and a low conductivity. These conductivity gradients and the corresponding

gradients in the local electromigration velocity of analytes produce a stacking/focusing phenomenon at the interfaces of enrichment (cathodic reservoir) and depletion (anodic reservoir) shocks. These shocks are net boundaries where the analyte can locate and thus concentrate. Based on a general analytical theory of CP [9,11], the various theoretically predicted mechanisms for CP of the BGE are governed by the two key parameters:

1/ an inverse Dukhin number $1/D_u$, which describes the ratio of bulk conductivity to surface conductivity, defined by $\frac{1}{D_u} = \frac{G_{bulk}}{G_\sigma} = \left(\frac{\nu_1 z_1 - \nu_2 z_2}{-2\nu_1 \sigma}\right) F h_n c_{0,r}$, where ν_i and z_i are respectively the mobility and the valence number of the ith ion (1 for the ion Na^+ or K^+ and 2 for the co-ion Cl^-), F is the Faraday number, h_n is the nanoslit height, σ is the surface charge and $c_{0,r}$ is the concentration of the co-ion in the reservoir.

2/ the velocity of the co-ion (to the wall charge) nondimensionalized by the electroosmotic velocity $\nu_2^* = \frac{\nu_2 z_2 F \eta}{\zeta_n \varepsilon}$, where ζ_n is the zeta potential value assumed to be uniform along the structure, η is the viscosity and ε is the permittivity.

At high $1/D_u$ values and low ν_2^*, values the concentrated analyte will stack at the entrance of the nanochannel in a regime called "CP without propagation" ($1/D_u \gg 1$) [11]. Such stacking could not be used for real applications of preconcentration since the analyte is confined in the vicinity of the nanochannel. On the opposite, at low inverse Dukhin number ($1/D_u \ll 1$), the analyte will stack at the sharp interface of enrichment shock (cathodic reservoir) or focus at the interface of depletion shock (anodic reservoir) in a regime called "propagating CP". We have previously shown based on computations [12] that an anionic analyte, such as fluorescein, diluted at low BGE concentration (down to 10µM), will concentrate in the cathodic reservoir in an

electrophoretically dominated regime. Such a very low ionic strength with high surface charge promotes a cathodic concentration profile unstable over time that corresponds to the propagating CP of the BGE (see Fig. 1(a)) [9]. This type of stacking "cathodic counter gradient focusing" (CCGF)[11,16] will be named here "Cathodic Focusing" (CF) to simplify.

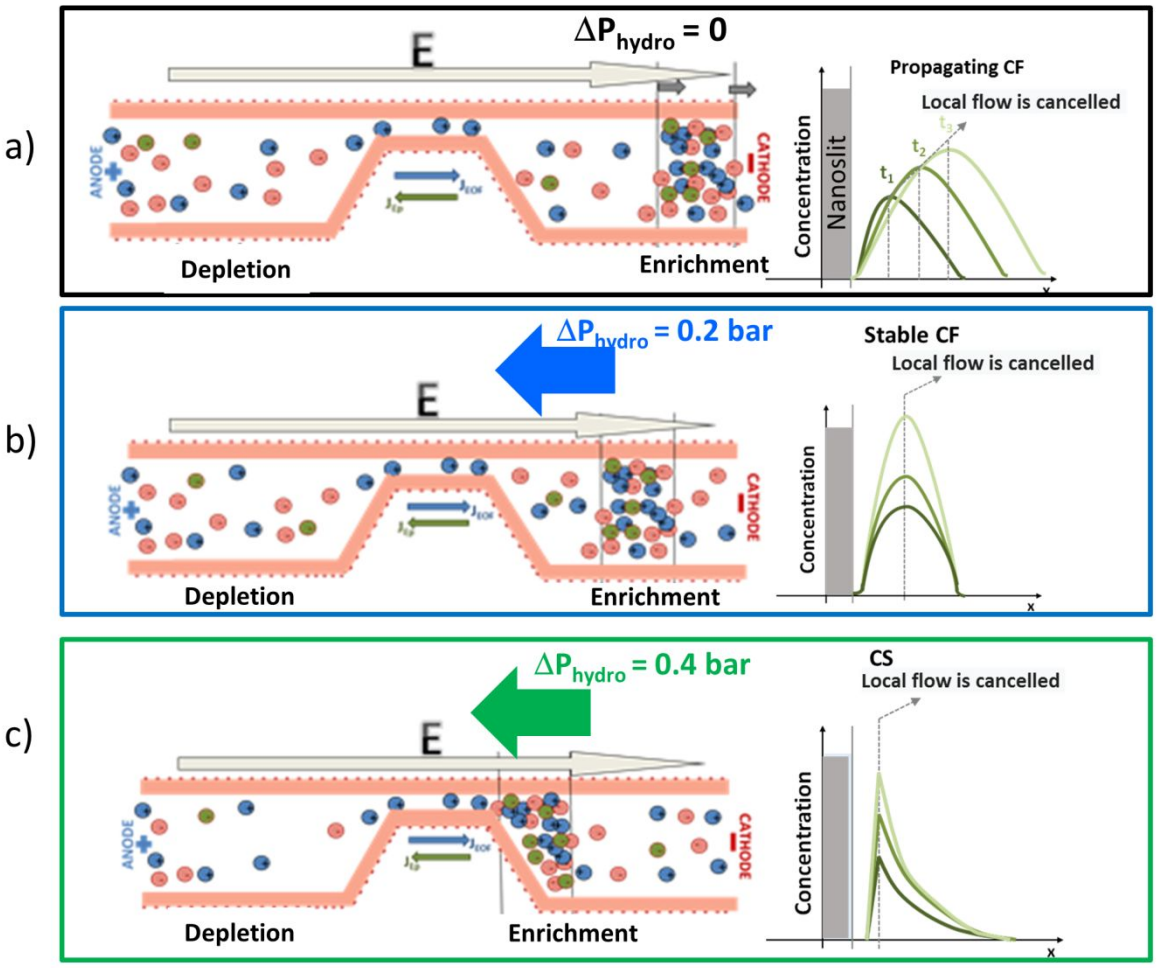

Figure 1. Cross-view of the micro/nano/micro (MNM) device with (a) a typical "propagating CF" profile observed for an anionic analyte stacking and moving at the enrichment shock with $v_2^* < 1$ *for conventional electropreconcentration (without any counter-pressure* $\Delta P_{hydro} = 0$*), (b) stabilization of the concentration frontline under the application of a low cathodic counter-pressure* ΔP_{hydro} *producing a stable*

CF regime and (c) at higher cathodic counter-pressure (for example ΔP_{hydro}= 4 bars), the profile is pushed towards nanoslit entrance producing a stacking CS regime.

Our simulations have also shown that a stable CF frontline can be obtained in a sharp transition region of surface charge, between propagating CF at high surface charge and stacking CS located at the nanochannel entrance at low surface charge. However, since the range of the two parameters (surface charge and electric field) to obtain this stable CF point is too narrow, only a few experiments have been reported. For example, Hluskou *et al* [30] have experimentally reported concentration of negatively charged BSA, with a dynamic characteristic of co-ionic species stacking on the enrichment shock, associated to a concentration factor of 100 after 200 seconds.

In order to stabilize the propagating modes at $^1/_{D_u} \ll 1$, we have previously proposed a pressure-assisted preconcentration protocol in which a hydrodynamic pressure is added to reduce (or enhance) the electroosmotic flow. This strategy has allowed a better control of the preconcentration frontline location[31]. Here, we will show that such low cathodic counter-pressure allows stabilization of the CF frontline on the enrichment shock (see Fig 1.b)). In the first part of the paper, pressure-assisted electropreconcentration of fluorescein sodium as a model anionic analyte will be presented. The role of the nanoslit length in the competition between electrophoretic velocity and the BGE velocity at the CP enrichment shock will be discussed based on experiments with different nanoslit lengths. The three different regimes of preconcentration (propagating CF –Fig.1a), stable CF – Fig.1b) and CS – Fig.1c)) observed at different electric field E and counter-pressure P can be reported on "E/P" diagram. We will show how this diagram varies as a function of the nature of BGE (KCl and NaCl) at low ionic strength. Finally, to evaluate the ability of such pressure-assisted protocol to concentrate negatively charged proteins, experiments

were realized with ovalbumin in HEPES. The E/P diagram for ovalbumin confirms the existence of a large range of parameters where a stable CF regime is obtained.

2. The role of the counter-pressure on the stabilization of the frontline

Pressure-assisted electro-preconcentration consists in applying an external hydrodynamic pressure ΔP_{hydro} that produces an additional flow called $J_{pressure}=J_P$ through the nanochannel. In addition to electroosmotic (J_{EOF}) and electrophoretic (J_{EP}) flows that are competing through the CP effect, this additional hydrodynamic flow (J_P) enables to shift the location of the analyte focal point in a direction that depends on the direction of the applied pressure [31]. The total flow is given by $J = J_{EOF} + J_{EP} + J_P$ where the additional hydrodynamic flow J_P can take positive or negative values. In the absence of a hydrodynamic pressure ($J_P=0$), we will use the notations "classical" or "conventional" to describe electropreconcentration.

Let's first describe classical electropreconcentration with a model BGE such as KCl and NaCl. At low ionic strength C_{BGE}=10µM and $\nu_2^* < 1$, a propagating frontline should be observed in the cathodic reservoir (Fig.1a). Zangle's theory allows predicting the location of the preconcentration frontline by comparing the nondimensionalized velocity of the analyte ν_i^* to the critical values $\nu_i^{*\,crit}$ for each region (nanochannel, enrichment zone and cathodic reservoir) [11]. When CP propagates, analytes can move inwards on either side of the enrichment shock if their mobility is low enough to travel in the direction of the bulk flow in the enrichment zone but high enough to travel against bulk flow in the reservoir following the condition: $\nu_{i,e}^{*\,crit} > \nu_i^* > \nu_{i,cr}^{*\,crit}$. Both critical velocities in the enrichment zone and in the cathodic reservoir are respectively $\nu_{i,e}^{*\,crit} = \nu_2^*$ and $\nu_{i,cr}^{*\,crit} = 1/D_u$. Supporting information SI.1 gives calculations of $1/D_u$ and ν_2^* for both KCl and NaCl as BGE, and shows that the condition $\nu_{i,e}^{*\,crit} > \nu_i^* > \nu_{i,cr}^{*\,crit}$ is always respected in

our experiments, predicting a stacking of fluorescein at the enrichment shock interface in the cathodic reservoir [11].

We describe now how pressure-assisted electropreconcentration will modify the propagating frontline. In the case of an additional pressure applied from the cathode to the anode (named "cathodic pressure"), such cathodic counter-pressure reduces the role of EOF flow by promoting the electrophoretic component. Increasing J_P at moderate values of pressure allows stabilization of the CF profile as function of time as described in Figure 1b). Such stable CF electropreconcentration regime is usable for applications and can produce high concentration rate whose value increases with time. At higher counter-pressure, the analyte is pushed towards the entrance of the nanochannel in a cathodic stacking CS regime (Fig.1c)).

3. Materials and methods

Glass chip fabrication including glass microstructuration and bonding has been previously extensively described by A-C. Louër *et al.* [31].

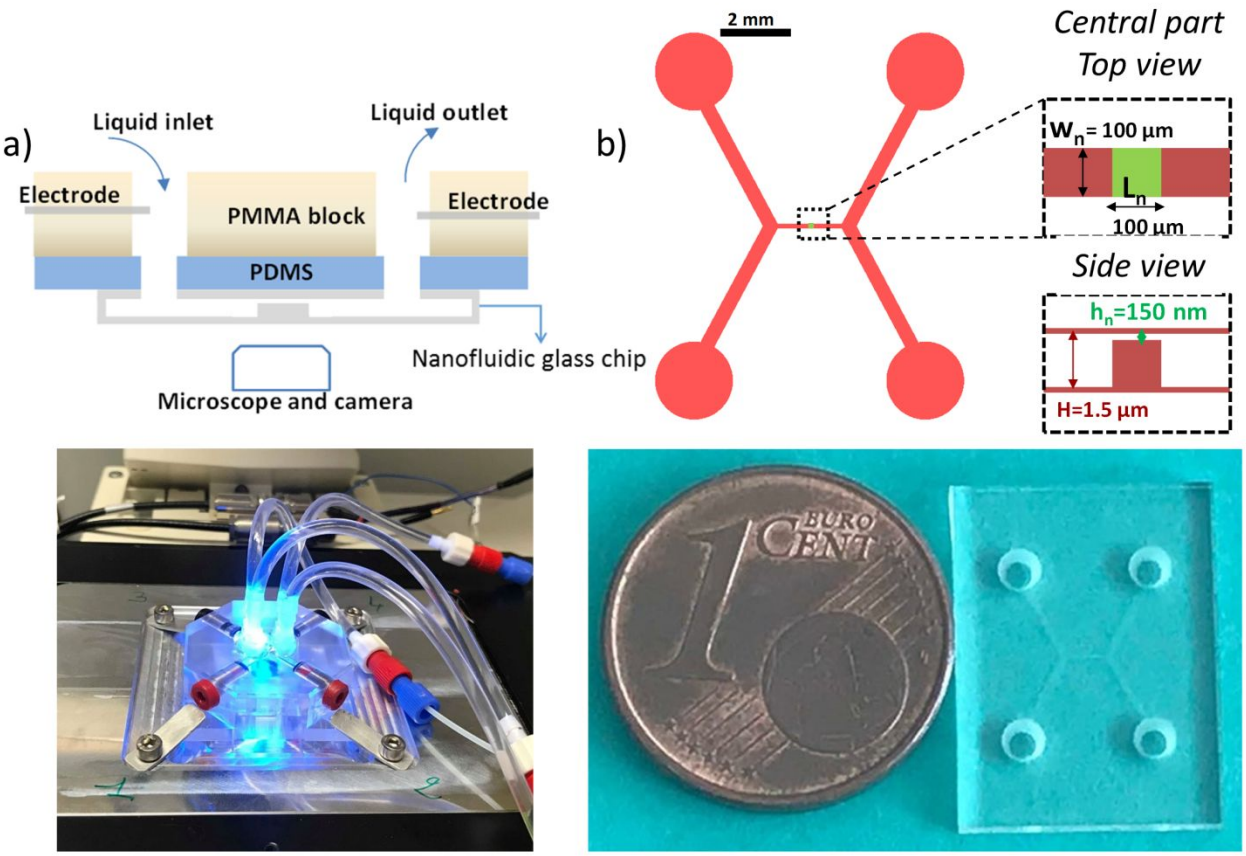

Figure 2. a) schematic of the PMMA chip holder allowing mounting the nanofluidic chip on the inverted microscope and picture of the holder recorded during experiment, b) schematic of the H chip with an integrated nanochannel and top-view photo of one nanofluidic glass chip.

Briefly, in the center of the "H" type 1 cm long chip, the nanoslit has a width *w* of 100 µm, a height h_n of 150 nm ± 10 nm and, depending of experiments, a length L of 500 µm or 100 µm (Figure 2). Both anodic and cathodic reservoirs are 1.5 µm deep.

For preconcentration experiments, fluorescein sodium salt from Sigma Aldrich was diluted at 10 µM in KCl or NaCl, whereas Texas red conjugated ovalbumin from Life Technologies was diluted in a 10 µM HEPES buffer. The external voltage was generated by a DC Keithley 238 power supply associated with a Keithley 7001 multiplexer. The additional hydrodynamic pressure was

applied through an ELVEFLOW® OB1 pressure generator, while sequential injection and flow stop were achieved with an ELVEFLOW® Multiplexer. Two cleaning processes were done before each experiment. First, each new chip was cleaned using the same protocol consisting in successive channels rinses with different solutions: 10 minutes with 1 M sodium hydroxide (NaOH) solution, 10 minutes with 0.1 M NaOH solution, 15 minutes with deionized water and 2 hours with the buffer solution. To get the same initial state before each application of electric field and pressure, an electro-cleaning was used based on three steps: i) applying 20 V for 2 minutes, ii) injection of the buffer for 10 minutes to renew the solution into the device, and finally iii) applying pressure in the four reservoirs for 10 minutes. The analyte solution is then injected with a syringe, in the four reservoirs. For imaging, an inverted fluorescent microscope (Axiovert 200, Zeiss), a mechanical shutter (Uniblitz VCMD1) and a CCD camera (Orca-ER, Hamamatsu) were used. Images were captured at regular intervals during preconcentration experiments (10 seconds during the first minute and then every 60 seconds). A Matlab® program was developed first to monitor the fluidic set-up during experiments and then to extract and analyze fluorescence profiles based on a preliminary calibration [31].

4. Results and discussion

4.1 Pressure-assisted electro-preconcentration of fluorescein: stabilization of CF regime:

The BGE concentration was kept at 10µM in all experiments to maintain the same CP buffer effect with $^1/D_u = 0.15$ and $\nu_2^* = 0.83$ for KCl and $^1/D_u = 0.18$ and $\nu_2^* = 0.83$ for NaCl. In order to study how both electric field E and pressure P can affect the stabilization of the CF regime, experiments with fluorescein have been performed at different external fields, E ranging from 5V/cm up to 80V/cm, and at several additional cathodic counter-pressures, P, ranging from 0 to 0.4 bars. Two different nanoslit lengths (L=500µm and L=100µm) have been studied.

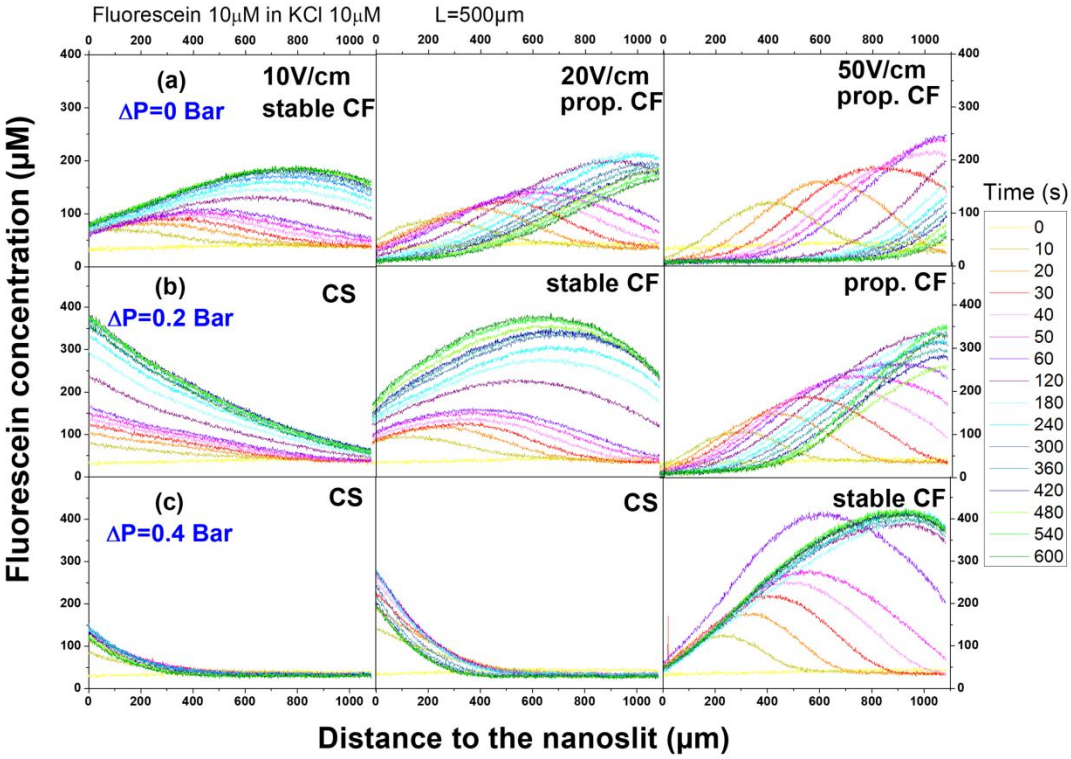

Figure 3. Electropreconcentration profiles of fluorescein diluted in KCl recorded for a nanoslit with L=500μm at several additional hydrodynamic pressures (a) ΔP=0 (conventional preconcentration), (b) ΔP = 0.2 bars and (c) ΔP =0.4 bars.

As shown in Figure 3a) for conventional cathodic preconcentration without any hydrodynamic counter-pressure (J_P=0), a stable CF profile is observed at low field (10V/cm), whereas an expected propagating CF is observed at higher fields 20V/cm and 50V/cm. One should note that the higher the field E is, the more propagating is the profile inside the cathodic reservoir. These experimental observations agree with the analytical calculations of Santiago [9-10] and Zangle [11], as well as with our previous simulations [12] at very low ionic strength, which both predict the cathodic focusing (CF) profile to be unstable over time especially for high electric fields and high surface charge.

Applying the cathodic counter-pressure ΔP allows stabilizing the fluorescein concentration profile as it can be observed in Figures 3b) and 3c). For example, at 20V/cm and ΔP=0.2 bar (Fig.3b)), the maximum of fluorescence intensity occurring at a distance of 600 µm from the nanoslit entrance remains quite constant as function of time even after 3 minutes. Similarly, at 50V/cm and ΔP= 0.4 bar (Fig.3c)), after 60 seconds, the CF peak stabilizes at a larger distance from the nanoslit, namely 950µm. Also, the concentration does not decrease for longer times which reflects a stable CF regime. This result shows that an additional hydrostatic pressure can be used to tune the buffer CP effect. This influence of additional flows on CP effect was also commented by Wang *et al.* [32] who has observed a propagating CP in their structures, while a stable CP region could be obtained when adding a transverse EOF flux in their "H shape" device. At low electric field, adding a high counter-pressure seems to constrain the preconcentration front toward the nanoslit in the same direction as the additional hydrostatic flow. At 10V/cm and ΔP = 0.2 bar (Fig.3b)), or 20V/cm and ΔP = 0.4 bar (Fig.3c)), the profile is stacked at the entrance of the nanoslit producing a CS regime. Similar experiments have been performed with chips that integrate shorter nanoslit (L = 100 µm – results not shown here – see Figure 6 in the following section). To conclude, adding a hydrodynamic counter-pressure from the cathodic side during fluorescein preconcentration allows manipulation and stabilization in space of the preconcentration frontline.

4.2 Time dependence of the localization of the preconcentration frontline:

Analyzing the evolution as function of time of both the peak location d_{max} and its corresponding concentration C_{max} appears also of great interest to determine the concentration rate C_{max}/C_0 and thus check the efficiency of the nanodevice to concentrate the analyte. Also, it allows checking the stability of the CF regime for intermediate values of counter-pressure. Figure 4 shows such an analysis of the experiments previously reported in Figure 3, for a nanoslit length L=500µm.

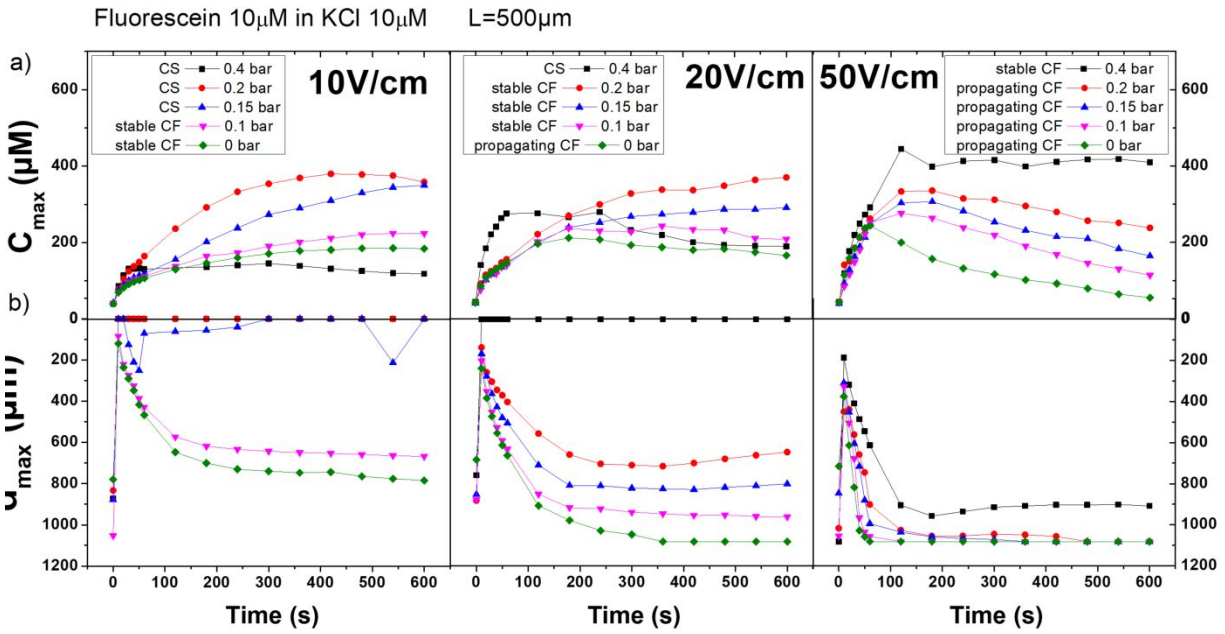

Figure 4. a) Evolution with time of C_{max} the maximum concentration of each profile for 10V/cm, 20V/cm and 50V/cm given in Figure 3, and b) corresponding time dependence of its location (distance from the nanoslit) for 10V/cm, 20V/cm and 50V/cm. A critical time of 200 s is observed to reach the stabilization.

As shown in Figure 4a) for E=20V/cm, adding a counter-pressure ΔP in the range 0.1-0.2 bar allows stabilization of the CF regime with a fixed localization at time higher than 200 seconds. One can observed a shift of the peak location from around 900 µm to 600 µm when ΔP increases from 0.1 to 0.2 bars. The optimal counter-pressure ΔP_{opt}= 0.2 bars produces the most stable CF regime with a concentration that increases with time to reach C_{max} = 450 µM after 10 minutes (C_{max}/C_0 = 45). At higher pressure (ΔP= 0.4 bars) the profile is stacked at the entrance of the nanoslit producing a CS regime as observed in Fig4.b) (dark curve). As shown in figure 4a), the higher the electric field is, the higher the optimal ΔP_{opt} is too with ΔP_{opt}= 0.1 bars for E=10V/cm, ΔP_{opt}= 0.2 bars for E=20V/cm and ΔP_{opt}= 0.4 bars for E=50V/cm.

However, since both fields 20V/cm and 50V/cm produce the same concentration rate C_{max}/C_0 of about 45, the best conditions of preconcentration using KCl as BGE are 20V/cm and ΔP_{opt}= 0.2 bars if one wants to minimize both E and P. However, it appears that the time transition to reach stabilization of the CF regime is shorter at 50V/cm as shown by the dark curves of figures 4a) and b) corresponding to 0.4 bar. The highest the field is, the higher P has to be fixed to stabilize the preconcentration frontline. The concentration rate reaches a limit as function of field since the enrichment shock is a weak shock due to relatively low electric fields across the interface between enrichment region and cathodic reservoir [11].

It is of great interest to study how the nature of the BGE can affect these preconcentration profiles. Similar experiments were done with NaCl as BGE ($^1/_{D_u}$= 0.18 and ν_2^* = 0.83 -see SI.1 for the calculations) for which a propagating regime is also predicted. With a higher inverse Dukhin number $^1/_{D_u}$ for NaCl compared to KCl, on should expect an easier stabilization of the propagating CF in this BGE.

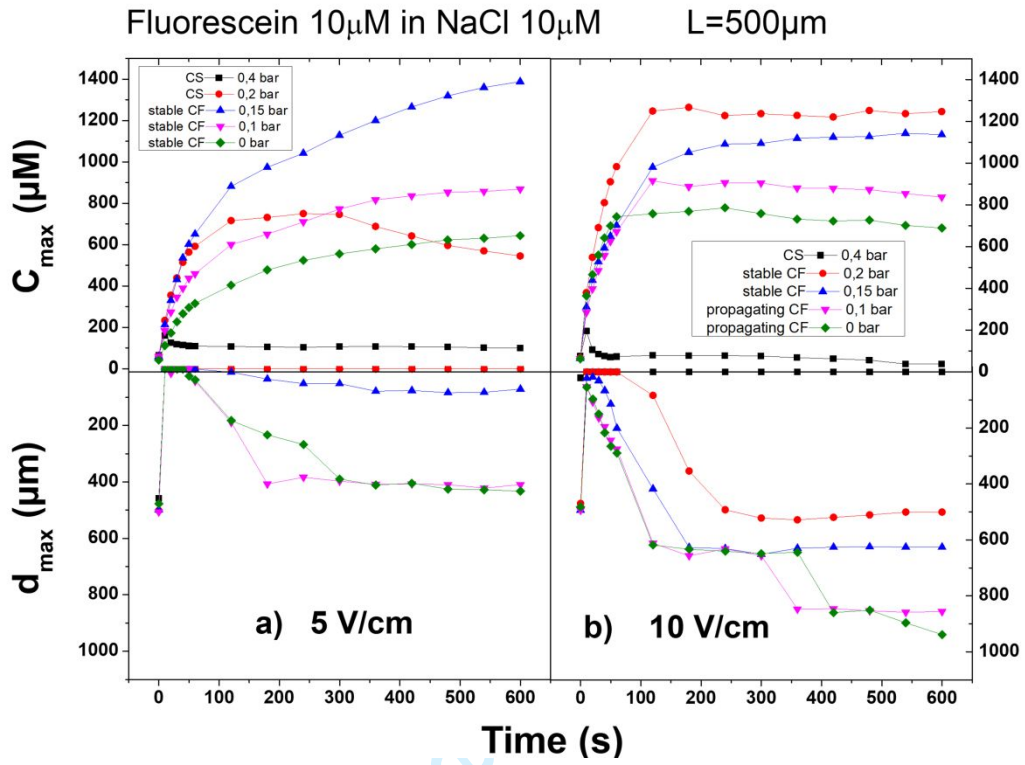

Figure 5. Evolution with time of C_{max} the maximum concentration of each profile for (a) 10V/cm, (b) 20V/cm and (c) 50V/cm for experiments performed in NaCl (L=500µm) and time dependence of its location (distance from the nanoslit) for (d) 10V/cm, (e) 20V/cm and (f) 50V/cm.

Figure 5 shows how both the peak location d_{max} and the maximum in concentration C_{max} evolve with time. Stabilization of the CF regime appears at lower electric fields, namely 5V/cm and 10V/cm, compared to KCl experiments. One can also observed the optimal ΔP_{opt} with ΔP_{opt}= 0.15 bars for E=5V/cm and ΔP_{opt}= 0.2 bars for E=10V/cm. For these optimal conditions, the localisation of the focal point ranges between 450µm and 500µm, 100µm closer to the nanoslit entrance than for KCl experiments. In addition, the concentration rate C_{max}/C_0 is largely enhanced with C_{max}/C_0=130 for E=5V/cm-ΔP_{opt}= 0.15 bars (blue curve in Figure 5.a)) and C_{max}/C_0=120 for E=10V/cm-ΔP_{opt}= 0.2 bars (red curve in Figure 5.b)). All these results confirm that stabilization of the propagating CF regime is easier in NaCl. This is not surprising since our analyte sodium

fluorescein diluted at 10µM contains as many Na^+ cations as the background electrolyte (NaCl – 10µM). Even if potassium can also exchange with sodium counter-ion in the KCl BGE, NaCl electrolyte appears here as a better BGE for stabilization of CF regime at low voltage. Looking at 10V/cm field and comparing left part of figure 4 and figure 5b), it appears that the NaCl BGE leads to stable CF until 0.15 bar associated to a higher C_{max}/C_0 preconcentration factor compared the KCl BGE. We assume that the sodium cations provide rapid exchanges between the NaCl BGE and the fluorescein. This situation offers a narrower and more fluorescent CF stable window in the preconcentration diagram. With KCl BGE, the bigger and slower potassium counter-ion will slightly change the polarisation of the fluorescein and it probably creates two distinct populations of fluorescein the first majority one with Na^+ and the other one with K^+. This configuration leads to broader but less fluorescent preconcentration plug during the CF because of the two distinct electrophoretic mobilities coming from K^+-fluorescein and from the Na^+-fluorescein.

4.3 "Electric field/Pressure" diagrams:

From all these experimental results at a unique ionic strength of 10µM, it is of great interest to build "electric field / pressure" diagrams, which were obtained in the following way. For each experiment, a classification of the different types (propagating CF, or stable CF, or CS) of preconcentration regimes obtained can be done. For each profile obtained, a point corresponding to one of the three regimes is located in an "electric field / pressure" diagram that will be named E/P diagram in the following.

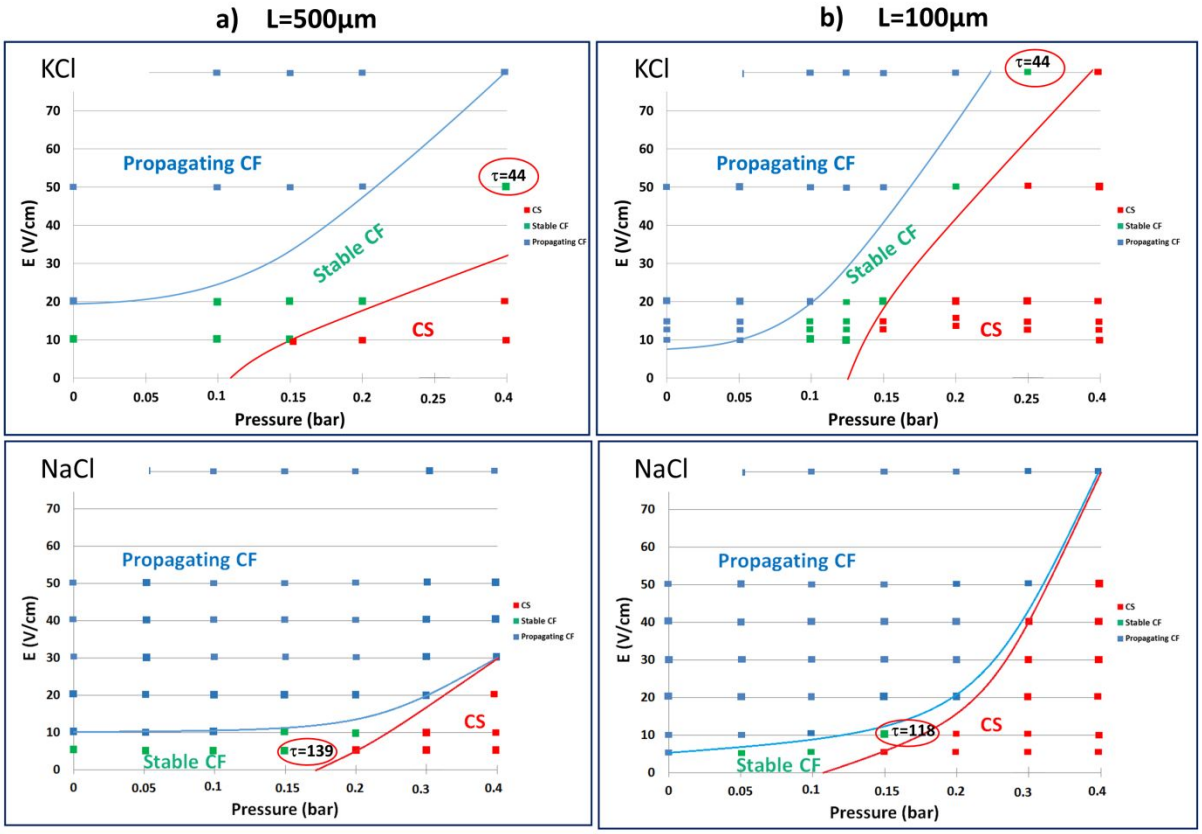

Figure 6. The "Electric field /Pressure" diagram established from Fluorescein electropreconcentration experiments using a chip that integrates a 150nm-high nanoslit with a length (a) L=500µm or (b) L=100µm and for the two BGE KCl and NaCl (C=10µM). Blue and red curves are guidelines to evidence the limit between each regime. The maximal value of the preconcentration rate $\tau=C_{max}/C_0$ is also reported in each diagram showing for each diagram the best couple of parameters (E, P).

These E/P diagrams allow observing the three regions that correspond to the three different preconcentration regimes, namely propagating CF (in blue), stable CF (in green) and CS (in red). Four E/P diagrams have been obtained for two different lengths of the nanoslit $L_{nanoslit}$= 500 µm (see Figure 6.a)) and $L_{nanoslit}$= 100 µm (see Figure 6.b)) in the two BGE solutions, KCl and NaCl. In these diagrams, the maximal value of the preconcentration rate $\tau=C_{max}/C_0$ has also been reported allowing a direct observation of the best couple (E, P) of parameters.

Whatever the nature of the buffer, it is observed that the short nanoslit L = 100 µm always leads to propagating regimes when no counter-pressure is added (ΔP=0 for conventional electropreconcentration). On the other hand, with long nanoslit (L = 500 µm), a stable CF regime can be obtained at ΔP = 0 and low field, namely 10V / cm for KCl and 5V / cm for NaCl. This is explained by a more pronounced CP effect for 500µm-long nanoslit. Moreover, the comparison between the diagrams established for KCl and for NaCl shows that the area of observation of the stable CF regime (in green) is shifted towards the weak electric fields for NaCl. Preconcentration rates obtained are also greater with NaCl than with KCl, as shown by the values circled in red on the 4 diagrams. With NaCl as background solution, it is therefore easy to stabilize CF regime at low electric field (< or = at 5V / cm) and low counter-pressure (< or = at 0.15 bar). These conditions produce the maximal value of the preconcentration rate $\tau=C_{max}/C_0 \sim 140$. The analyst will thus have to choose between a broader stability window or a high preconcentration factor. This choice will be driven by the instrumentation, namely the speed of the camera or the sensitivity of the optical sensor. The initial concentration of the analyte is also another main parameter to consider before choosing the nature of the BGE. For trace analysis, a fluorescence optical sensor with high spatial resolution will be probably preferred since high preconcentration rate is required. In that case, NaCl appears as the best BGE. On the other hand, with analyte at higher concentration, with KCl as BGE, the stability of the preconcentration plug could be reached faster because of the wider stability domain (see Figure 6). Once again, these results underline the interdependence between the choice of the BGE and the quality of the analysis by electrophoretic methods. In other words, similarly as the popular free zone electrophoresis, electropreconcentration with a microfluidic device bearing a nanoslit requires cautious adjustments of the BGE composition regarding to the sample composition and its available quantity.

4.4 Pressure-assisted electro-preconcentration of Ovalbumin:

Chicken ovalbumin is a 45 kDa protein that is the major component of egg white. Fluorescent ovalbumin can be used as endocytic tracers [33-35] and to estimate the size of the transport pathways of micro-vessels [36]. It is also used in various research fields such as studying the structure and functionality of serpins, and proteomics (egg yolk ovalbumin is frequently used as a molecular marker for calibration of electrophoresis gels) or immunology frequently used to stimulate an allergic reaction on test subjects [37-38].

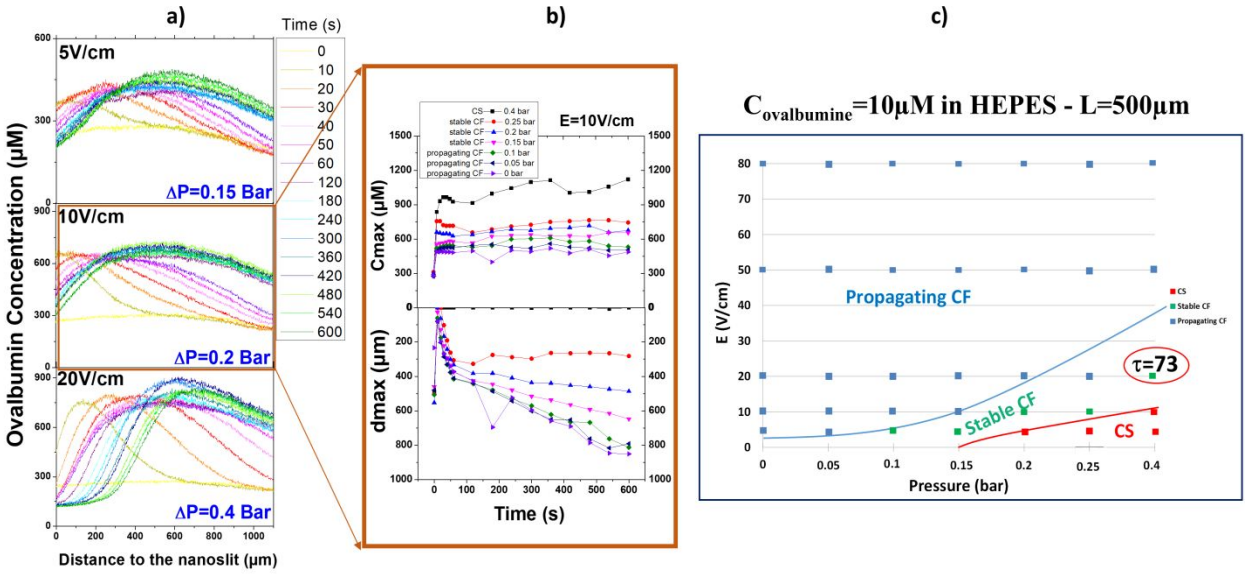

Figure 7. (a) Electropreconcentration profiles of ovalbumin diluted at 10µM in HEPES at 10µM recorded for a nanoslit with L=500µm at different coupled E/P that produce stable CF regimes, (b) Evolution with time of C_{max} the maximum concentration of each profile for 10V/cm and 0.2 bars, and time dependence of its location (distance from the nanoslit), (c) The "Electric field /Pressure" diagram established from ovalbumin electropreconcentration experiments showing at 20V/cm and 0.4 bars the maximal rate $\tau=C_{max}/C_0=73$.

In order to validate the pressure-assisted protocol for a more applicative protein that our previous model molecule of sodium fluorescein, experiments were carried out with ovalbumin. For these experiments, only 500µm-long nanoslit were used as they produce the highest CP effect of the BGE in the MNM structure. Here, the background solution chosen was a real buffer frequently used in analytical chemistry, the organic zwitterionic HEPES compound. Unlike phosphate and bicarbonate buffers, this HEPES buffer solution helps maintaining the structure and function of proteins at low temperatures. Moreover, the use of zwitterionic buffers as BGE allow the application of high separation voltages while maintaining a low current. Ovalbumin was thus diluted at a concentration of 10 µM in a 10 µM HEPES solution. Ovalbumin was marked with the Texas Red marker whose maximum emission and absorption wavelengths are respectively λ=615nm and 596nm.

Similarly, just as sodium fluorescein, ovalbumin concentrates in the cathodic reservoir. For clarity, only profiles corresponding to a stable CF regime have been reported here in Figure 7a). Despite the high CP effect in HEPES due to the long nanoslit (L = 500µm), propagating regimes are always observed using conventional electrophoresis at $\Delta P = 0$. Quite high counter-pressure must be applied, from 0.15 bar (with E = 5V / cm) to 0.4 bar (with E = 20V / cm) to stabilize the CF regime. On the other hand, similarly as for our previous experiments with NaCl as background salt, it is not necessary to apply high electric fields, as shown in the diagram obtained (Figure 7.b). Obtaining the stable CF regime for a protein of interest such as ovalbumin at low-electric field is very interesting in terms of applications. The maximal concentration rate for ovalbumin of about $\tau = C_{max}/C_0 = 73$ after several minutes is also promising. All those experiments carried out with ovalbumin confirm the great interest of adding an additional counter-pressure to obtain quickly

stable CF regimes over time inside a micro/nano/micro fluidic device able to concentrate such derivatized biomacromolecule at high concentration rate.

Conclusion

In this work, a pressure-assisted preconcentration protocol in which a hydrodynamic pressure is added to reduce the electroosmotic flow is shown to stabilize propagating modes at $1/D_u \ll 1$. Low cathodic counter-pressure allows stabilization of the CF frontline on the enrichment shock whereas higher counter-pressure produces CS stacking regime at the nanoslit entrance. The three different preconcentration regimes (propagating CF, stable CF and CS) observed at different electric field E and counter-pressure P for fluorescein sodium (C=10µM) can be reported on an original "E/P" diagram. The role of the nanoslit length in the competition between electrophoretic velocity and the BGE velocity at the CP enrichment shock can be easily evidenced on the corresponding "E/P" diagram. It is shown that higher P values are needed for CF stabilization with shorter nanoslit ($L_{nanoslit}$= 100 µm) with a weaker CP effect, compared to longer slit ($L_{nanoslit}$= 500 µm). The stable CF region in such "E/P" diagram is also changing as function of the nature of BGE (KCl and NaCl) with an easier stabilization at low E for NaCl and higher preconcentration rates. Finally, the ability of such pressure-assisted protocol to concentrate negatively charged proteins has been tested with 10µM ovalbumin in HEPES and the corresponding E/P diagram for ovalbumin confirms the existence of a stable CF regime at low electric field.

Acknowledgments

All authors would like to thank ANR for the financial support (DIFLUSEL and NANOCODE).

References

(1) L. Gervais, N. D. Rooij, and E. Delamarche, *Adv. Mater.*, *vol. 23*, no. 24, pp. H151-H176, **2011**.
(2) H. Virk, S. Kaur, and G. Randhawa, *Environ. Int.*, *27*, 359-362, **2001**.
(3) J. A. Quinn, J. L. Anderson, W. S. Ho, and W. J. Petzny, *Biophys. J.*, *12*, 990-1007, **1972**.
(4) Y. Wang, M. Choi, and J. Han, *Anal. Chem.*, *76*, 15, 4426-4431, **2004**.
(5) A. Asif and D. Chung, *Electrophoresis*, *26*, 3, 668-673, **2005**.
(6) Q. Pu, J. Yun, H. Temkin, and S. Liu, *Nano Letters*, 4, 1099–1103, **2004**.
(7) V. Kašicka, *Electrophoresis*, 41, 10-35, **2020**.
(8) A. Plecis, R.B. Schoch, and P. Renaud, *Nano Letters* 5(6), 1147-1155, **2005**.
(9) Ali Mani, Thomas A. Zangle, and Juan G. Santiago, *Langmuir* 25, 3898-3908, **2009**.
(10) Thomas A. Zangle, Ali Mani, and Juan G. Santiago, *Langmuir* 25, 3909-3916, **2009**.
(11) Thomas A. Zangle, Ali Mani, and Juan G. Santiago, *Chem. Soc. Rev.* 39, 1014, **2010**.
(12) A. Plecis, C. Nanteuil, A.-M. Haghiri-Gosnet, and Y. Chen, *Anal. Chem.*, 80, 9542–9550, **2008**.
(13) S. J. Kim, Y. Song, and J. Han, *Chem. Soc. Rev.* 39, 912, **2010**.
(14) C.Wang, Y. Wang, Y. Zhou, Z.Q. Wu and X.H. Xia, *Anal. Bioanal Chem.,* 411, 4007-4016, **2019**.
(15) L.M. Fu, H.H. Hou, P.H. Chiu and R.J. Yang, *Electrophoresis*, 39, 289-310, **2018**.
(16) S. A. Hong, Y. J. Kim, S. J. Kim and S. Yang, *Biosens. Bioelectron*, 107, 103-110, **2018**.
(17) S. J. Lee, J. Lee and K. Kim, *Anal. Biochem*, 557, 13-17, **2018**.
(18) J. Choi, S. Baek, H. C. Kim, J-H. Chae, Y. Koh, S. W. Seo, H. Lee and S.J. Kim, *BioChip J.,* 14(1), 100-109, **2020**.
(19) C-C Lin, J-L. Hsu and G-B. Lee, *Microfluid Nanofluid*, 10, 481-511, **2011**.
(20) W. Ouyang and J. Han, *Proc Natl Acad Sci USA*, 116(33), 16240-16249, **2019**.
(21) R. Bharaswaj and J.G. Santiago, *J. Fluid. Mech.* 543, 57, **2005**.
(22) J. M. Sustarich, B.D. Storey and S. Pennathur, *Phys. Fluids* 22, 112003, **2010.**
(23) L. Ouyang, Q. Liu, H. Liang, *J. Sep. Sci.,* 40, 789-797, **2017**.
(24) D. W. Inglis, E. M. Goldys, and N. P. Calander, *Angew. Chem. Int.* 50, 7546 –7550, **2011**.
(25) W.L. Hsu, D.J. Harvie, M.R. Davidson, H. Jeong, E.M. Goldys and D.W. Inglis, *Lab. Chip* 14, 3539, **2014**.
(26) W.L. Hsu, D.W. Inglis, M. A. Startsev, E. M. Goldys, M.R. Davidson, *Anal. Chem*., 86, 8711-8718, **2014**.
(27) W. Ouyang, Z. Li, J. Han, *Anal. Chem*., 90(19), 11366-11375, 2018
(28) M.A. Startsev, M. Ostrowski, E.M. Goldys and D.W. Inglis, *Electrophoresis*, 38, 335-341, **2017**.
(29) M.A. Startsev, D.W. Inglis, M.S. Baker and E.M. Goldys, *Anal. Chem.,* 85(15), 7133-7138, **2013**.
(30) D. Hlushkou, R. Dhopeshwarkar, R.M. Crooks, U. Tallarek, *Lab. Chip* 8, 1153-1162, **2008**.
(31) A-C. Louër, A. Plecis, A. Pallandre, J-C. Galas, A. Estevez-Torres and A.-M. Haghiri-Gosnet, *Anal. Chem.*, 85, 79487956–9550, **2013**.
(32) Y. Wang, A. Stevens, and J. Han, *Anal. Chem.*, 77, 4293–4299, **2005.**
(33) M.S. Swanson and R.R. Isberg, *Infect Immun*, 64(7), 2585-2594, **1996**.

(34) L.M. Refolo, K. Sambamurti, S. Efthimiopoulous, M.A. Pappolla and N.K. Robakis, *J Neurosci Res,* 40(5), 694-706, **1995**.
(35) G. Grieco, V. Janssens, H.P. Gaide Chevronnay *et al., Sci. Rep,* 8, 14133, **2018**.
(36) J.E. McNamee and M.B. Wolf, *Microcirculation,* 5(4), 275-280, **1998**.
(37) J. Golias, M. Schwarzer, M. Wallner, M. Kverka, H. Kozakova et al. *PLOS ONE*, 7(5): e37156, **2012**.
(38) T. Hilmenyuk, I. Bellinghausen, B. Heydenreich, A. Ilchmann, M. Toda, S. Grabbe, and J. Saloga, *Immunology*, 129(3), 437-445, **2010**.

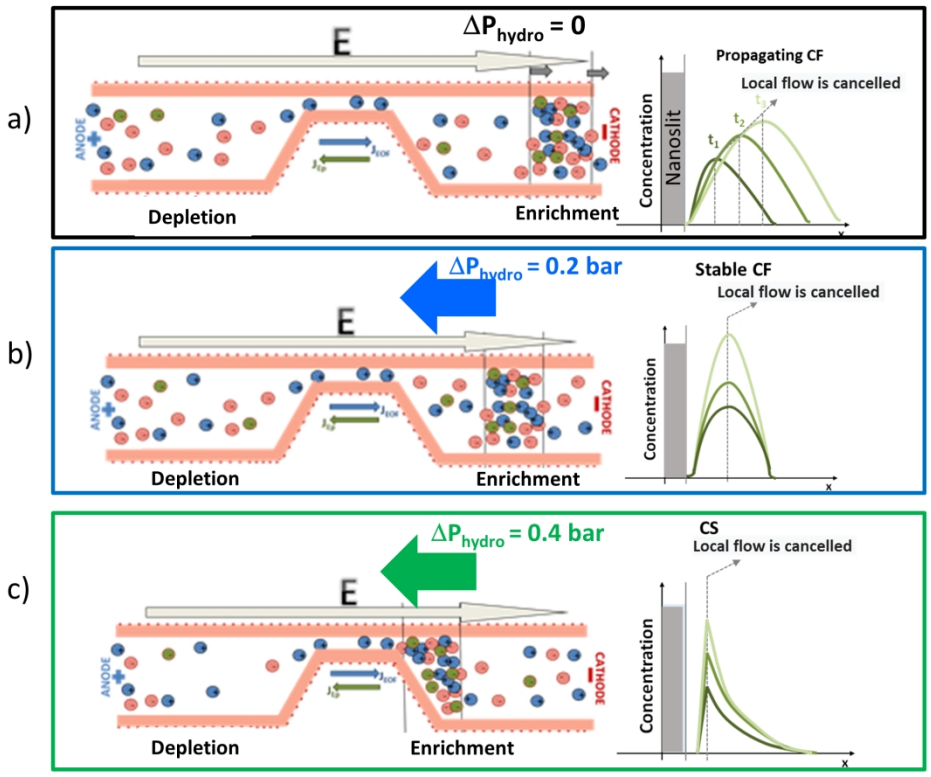

Figure 1. Cross-view of the micro/nano/micro (MNM) device with (a) a typical "propagating CF" profile observed for an anionic analyte stacking and moving at the enrichment shock with $v_2^* < 1$ for conventional electropreconcentration (without any counter-pressure $\Delta P_{hydro} = 0$), (b) stabilization of the concentration frontline under the application of a low cathodic counter-pressure ΔP_{hydro} producing a stable CF regime and (c) at higher cathodic counter-pressure (for example $\Delta P_{hydro} = 4$ bars), the profile is pushed towards nanoslit entrance producing a stacking CS regime

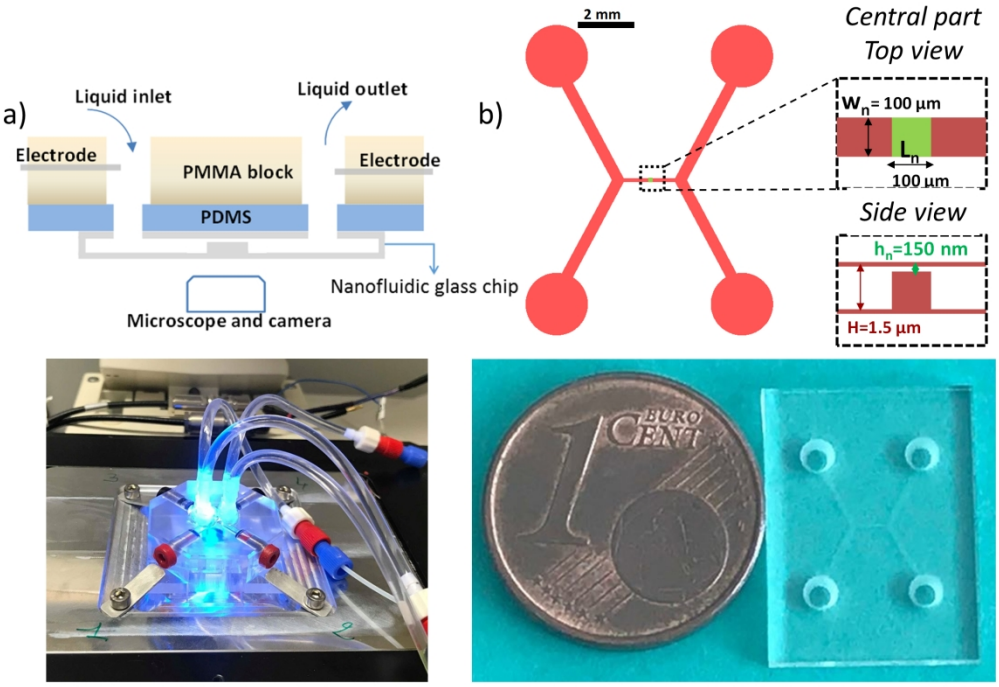

Figure 2. a) schematic of the PMMA chip holder allowing mounting the nanofluidic chip on the inverted microscope and picture of the holder recorded during experiment, b) schematic of the H chip with an integrated nanochannel and top-view photo of one nanofluidic glass chip.

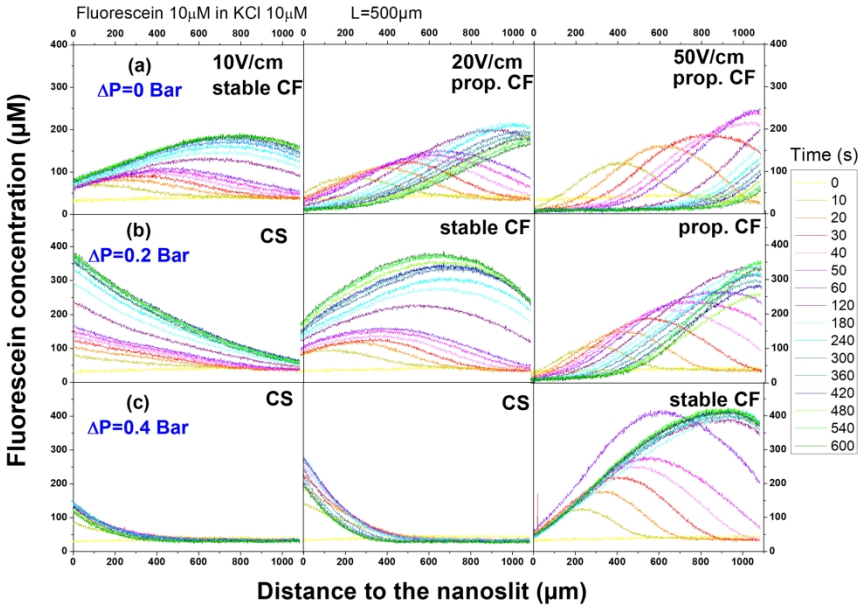

Figure 3. Electropreconcentration profiles of fluorescein diluted in KCl recorded for a nanoslit with L=500μm at several additional hydrodynamic pressures (a) ΔP=0 (conventional preconcentration), (b) ΔP = 0.2 bars and (c) ΔP =0.4 bars.

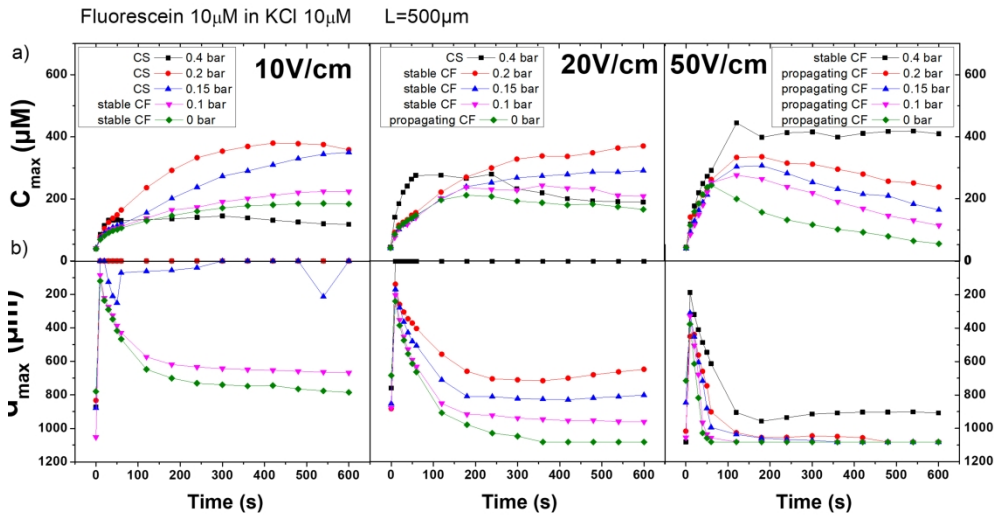

Figure 4. a) Evolution with time of C_{max} the maximum concentration of each profile for 10V/cm, 20V/cm and 50V/cm given in Figure 3, and b) corresponding time dependence of its location (distance from the nanoslit) for 10V/cm, 20V/cm and 50V/cm. A critical time of 200 s is observed to reach the stabilization.

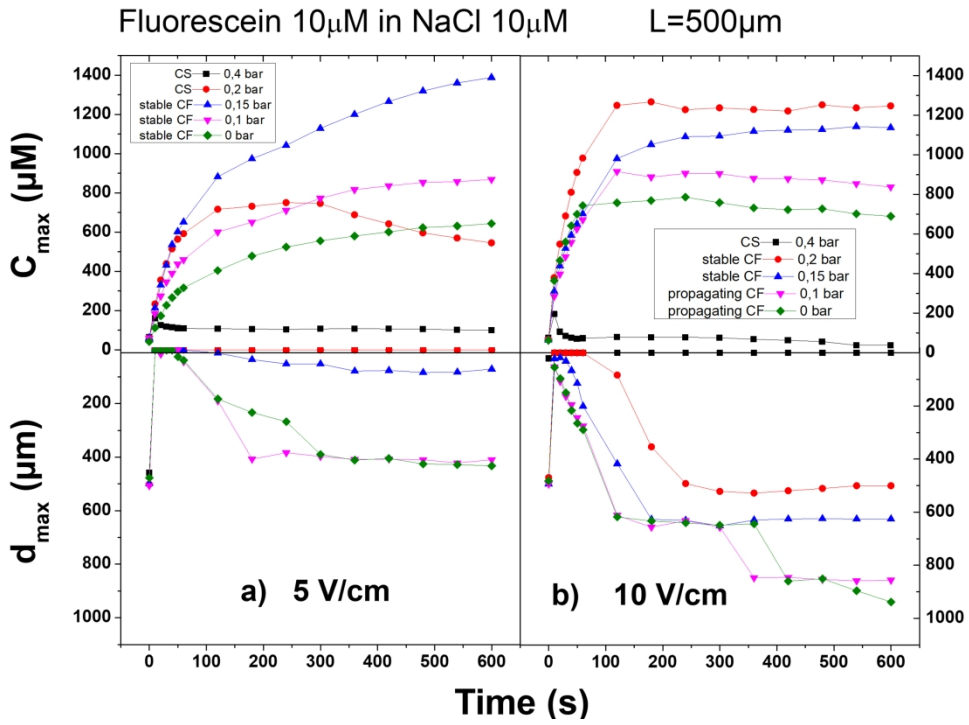

Figure 5. Evolution with time of C_{max} the maximum concentration of each profile for (a) 10V/cm, (b) 20V/cm and (c) 50V/cm for experiments performed in NaCl (L=500µm) and time dependence of its location (distance from the nanoslit) for (d) 10V/cm, (e) 20V/cm and (f) 50V/cm.

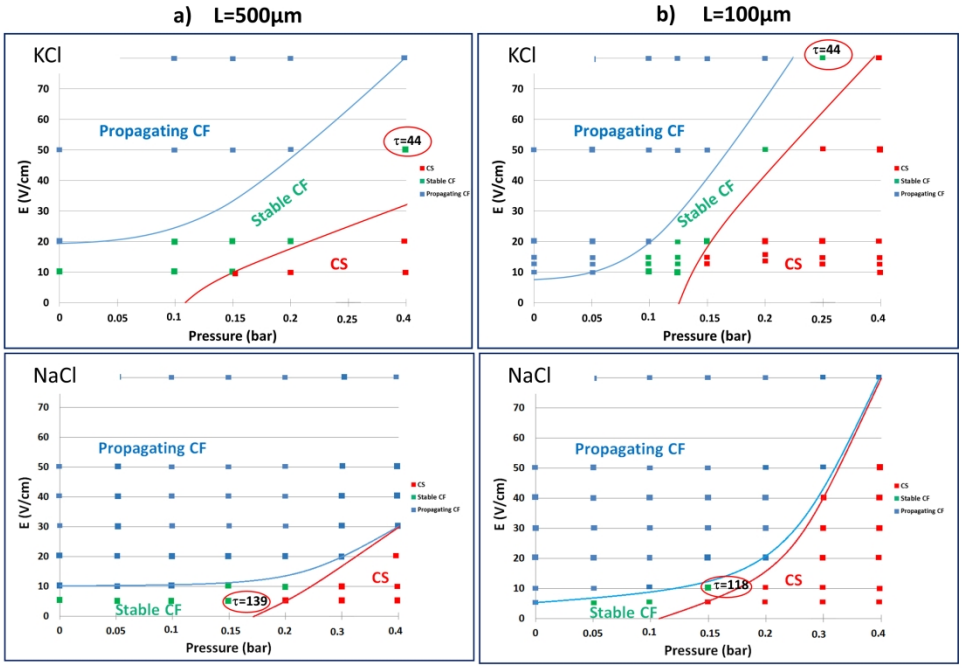

Figure 6. The "Electric field /Pressure" diagram established from Fluorescein electropreconcentration experiments using a chip that integrates a 150nm-high nanoslit with a length (a) L=500µm or (b) L=100µm and for the two BGE KCl and NaCl (C=10µM). Blue and red curves are guidelines to evidence the limit between each regime. The maximal value of the preconcentration rate $\tau=C_{max}/C_0$ is also reported in each diagram showing for each diagram the best couple of parameters (E, P).

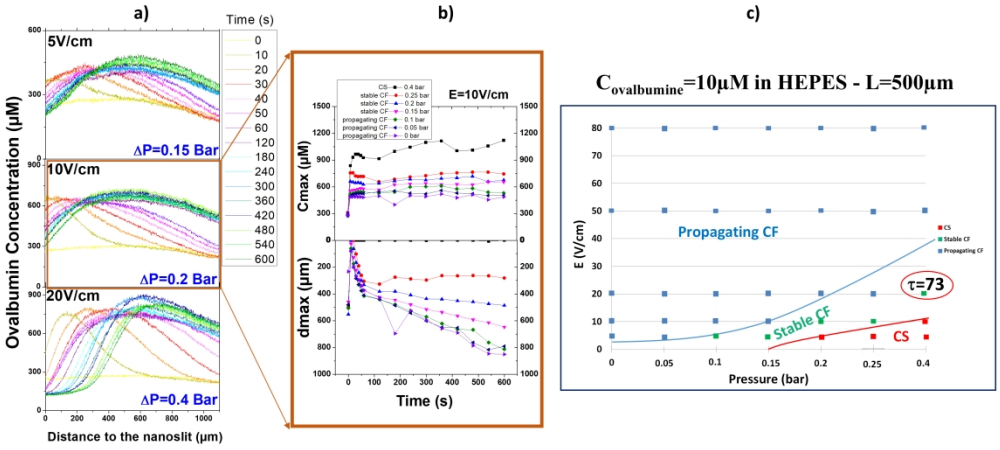

Figure 7. (a) Electropreconcentration profiles of ovalbumin diluted at 10µM in HEPES at 10µM recorded for a nanoslit with L=500µm at different coupled E/P that produce stable CF regimes, (b) Evolution with time of Cmax the maximum concentration of each profile for 10V/cm and 0.2 bars, and time dependence of its location (distance from the nanoslit), (c) The "Electric field /Pressure" diagram established from ovalbumin electropreconcentration experiments showing at 20V/cm and 0.4 bars the maximal rate $\tau=C_{max}/C_0=73$

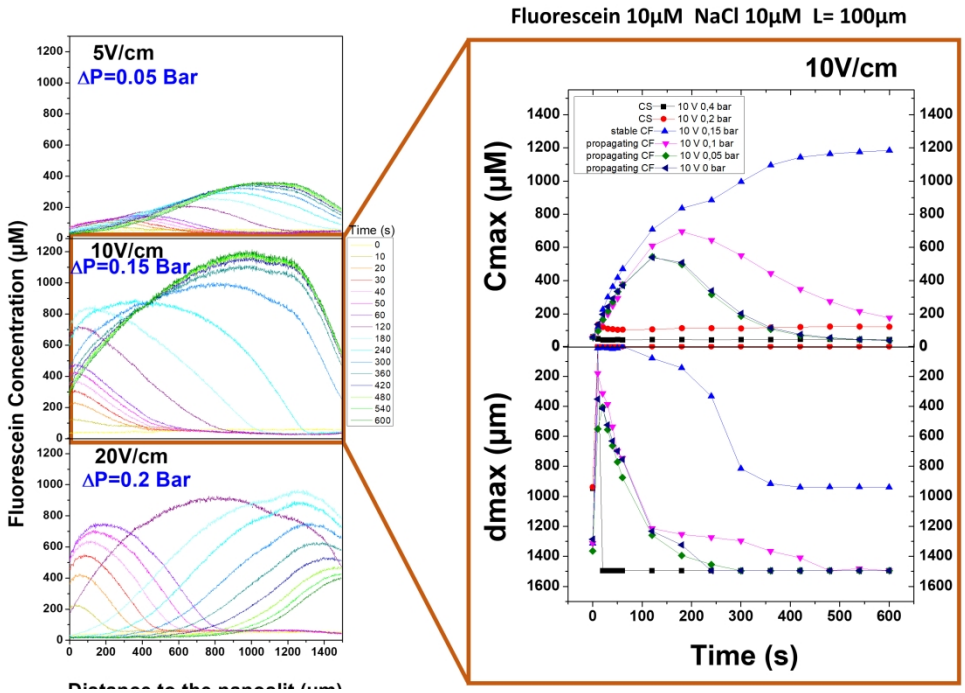

Figure S1.2 - Electropreconcentration profiles recorded at different voltages and different additional hydrodynamic pressures in NaCl 10µM with a chip that integrates a 100µm long nanoslit (a) 5 V/cm, 0.05 bar (b) 10 V/cm, 0.15 bar and (c) 20 V/cm, 0.2 bar; (d) at 10 V/cm, the evolution with time of the maximal concentration C_{max} and time dependence of the corresponding distance from the nanoslit d_{max}.